Fu et al. *NPG Asia Materials* (2022) 14:99
https://doi.org/10.1038/s41427-022-00444-x

NPG Asia Materials

ARTICLE Open Access

A cyclic heptapeptide-based hydrogel boosts the healing of chronic skin wounds in diabetic mice and patients

Zhe Fu[1], Huiling Sun[1], Yutong Wu[1], Chao Li[1,2], Yinglei Wang[1], Yixiang Liu[3], Yilin Li[1], Junxu Nie[4], Dandan Sun[1], Yingxuan Zhang[1], Naixin Liu[1], Kun Guo[1], Saige Yin[1], Qiuye Jia[1], Ying Yang[4], Li He[5], Ying Wang[3] and Xinwang Yang[1,2]

Abstract

The combined use of peptides, nanomaterials, and hydrogels is a promising strategy for chronic skin wound healing, which remains a huge clinical challenge. Here, we optimized the RL-QN15 peptide, which was shown to be a pro-healing drug candidate in our previous research, to obtain the cyclic heptapeptide ($Cy_{RL\text{-}QN15}$) with considerable therapeutic potency against skin wounds. Furthermore, a Zn^{2+}-crosslinked sodium alginate (ZA) hydrogel containing hollow polydopamine (HPDA) nanoparticles loaded with $Cy_{RL\text{-}QN15}$ ($HPDAlCy_{RL\text{-}QN15}$/ZA hydrogel) was prepared and characterized, which significantly enhanced the pro-healing potency of $Cy_{RL\text{-}QN15}$. At the cellular level, this nontoxic hydrogel accelerated the proliferation, migration, tube formation, and scratch healing of skin cells, regulated the secretion of cytokines from macrophages, directly scavenged free radicals, and decreased reactive oxygen species. Moreover, the $HPDAlCy_{RL\text{-}QN15}$/ZA hydrogel significantly accelerated the healing of full-thickness skin wounds in type 2 diabetic mice by promoting the transition of macrophages to the M2 phenotype to reduce inflammation and cause re-epithelialization, formation of granulation tissue, deposition of collagen, and angiogenesis. Of note, the hydrogel also facilitated wound healing of diabetic patient skin cultured ex vivo. Overall, the $HPDAlCy_{RL\text{-}QN15}$/ZA hydrogel presents a novel therapeutic strategy for clinical chronic skin wound (diabetic ulcer) healing.

Introduction

Wound healing is a complex physiological process that maintains the structural integrity of the body and consists of hemostasis, inflammation, proliferation, and remodeling stages[1,2]. Wounds that fail to heal within a normal time frame are considered chronic wounds. Chronic wounds affect 0.2% to 1% of the population in developed countries, posing an increasing health and economic burden on society[3]. At present, chronic wound treatment lacks effective targeted therapies, focusing instead on optimizing controllable healing factors[4,5]. Therefore, exploring innovative intervention strategies to promote chronic skin wound healing remains essential.

Various novel interventions have been developed for chronic skin wounds, including the use of bioactive peptides, hydrogels, nanomaterials, and tissue engineering. In particular, bioactive peptides, hydrogel dressings, and nanomaterials have received considerable attention[6,7]. Several bioactive peptides derived from amphibian skin, such as OA-GL12, cathelicidin-OA1, cathelicidin-NV, and RL-QN15, have shown significant potential as novel pro-healing agents in the treatment of skin wounds[8–12]. A variety of biomaterials (e.g., hydrogels, nanofibers, and

Correspondence: Ying Yang (yangying2072@126.com) or Li He (drheli2662@126.com) or Ying Wang (wangying_814@163.com) or Xinwang Yang (yangxinwanghp@163.com)
[1]Department of Anatomy and Histology & Embryology, Faculty of Basic Medical Science, Kunming Medical University, Kunming, Yunnan 650500, China
[2]School of Pharmaceutical Science & Yunnan Key Laboratory of Pharmacology for Natural Products, Kunming Medical University, Kunming, Yunnan 650500, China
Full list of author information is available at the end of the article
These authors contributed equally: Zhe Fu, Huiling Sun, Yutong Wu, Chao Li

films) have also been used in the treatment of chronic wounds[13]. Hydrogels are three-dimensional (3D) networks formed by cross-linking hydrophilic polymer chains, with properties similar to those of the extracellular matrix (ECM). They are considered ideal scaffolds for wound healing due to their ability to absorb wound exudates, maintain a moist environment, and promote fibroblast proliferation and keratinocyte migration[14,15]. Sodium alginate (SA) consists of different ratios of β-1,4-linked repeating units of D-mannuronic acid (M) and L-glutamine (G)[16]. The high L-glutamine (G) block content of alginate enables the formation of an insoluble gel network by building bridges in the polymer network with divalent cations such as Zn^{2+}[17]. In addition, Zn^{2+} is an essential element for cell proliferation and angiogenesis and has shown excellent results in chronic skin wound healing[18]. Nanomaterials have been widely used in wound repair due to their unique surface properties, physiological activities, adjustable porous structure, outstanding biocompatibility, and drug loading ability[19]. Hollow polydopamine (HPDA) nanoparticles exhibit excellent surface permeability, load-carrying capacity, antioxidant activity, and controllable morphology, thus representing an ideal drug delivery system for chronic skin wound healing[20]. Therefore, incorporating peptides, nanomaterials, and hydrogels to create combination agents will lead to novel strategies for the treatment of chronic skin wounds. At present, however, relevant reports on skin wound healing remain scarce.

Optimization of existing bioactive peptides is an effective approach for developing novel agents, such as ziconotide, exenatide, bivalirudin, and captopril[21,22]. We previously identified a novel pro-healing peptide RL-QN15 from frog skin secretions, which contains intramolecular disulfide bonds without posttranslational modifications[23]. At low concentrations, RL-QN15 showed remarkable therapeutic potential in the healing of acute wounds, chronic wounds, skin fibrosis, oral ulcers, and full-thickness skin wounds in pigs[10]. We also developed a novel strategy to promote dermal wound healing by loading RL-QN15 into HPDA nanoparticles, which increased the pro-healing ability of the peptide[19]. However, further refinement of the RL-QN15 structure is important to reduce costs and increase activity and thus facilitate the development of novel pro-healing drugs.

In the current study, we optimized the structure of RL-QN15 and obtained a shorter cyclic heptapeptide ($Cy_{RL\text{-}QN15}$) with excellent skin wound healing activity. Furthermore, we successfully prepared and characterized a Zn^{2+} cross-linked SA hydrogel containing HPDA nanoparticles loaded with $Cy_{RL\text{-}QN15}$ (HPDAlCy$_{RL\text{-}QN15}$/ZA hydrogel) for chronic skin wound healing. At the cellular level, this nontoxic hydrogel accelerated the proliferation, migration, tube formation, and scratch healing of skin cells, regulated the secretion of cytokines from macrophages, directly scavenged free radicals, and decreased reactive oxygen species (ROS). The HPDAlCy$_{RL\text{-}QN15}$/ZA hydrogel also showed excellent therapeutic effects on full-thickness diabetic skin wounds in mice and full-thickness ex vivo foot skin wounds from diabetic patients. This study presents a prospective HPDAlCy$_{RL\text{-}QN15}$/ZA hydrogel for chronic skin wound healing and emphasizes the potential of combined therapy based on peptides, nanomaterials, and hydrogels for the clinical treatment of chronic skin trauma.

Experimental section

Animal ethics statement and informed consent

Male Kunming and C57BL/6 mice (20–24 g, 6–8 weeks old) were purchased from Hunan SJA Laboratory Animal Co., Ltd. (Hunan, China). All animal care and handling procedures were approved by and followed the requirements of the Ethics Committee of Kunming Medical University (kmmu20220069).

All human skin samples were obtained with informed consent from diabetic patients undergoing amputation surgeries at the Department of Endocrinology, Affiliated Hospital of Yunnan University (Kunming, Yunnan, China). Skin collection was approved by the Ethics Committee of the Affiliated Hospital of Yunnan University (2021103). Informed consent confirmed that the patients voluntarily donated their skin for wound healing research with no financial payment. This research abides by the Declaration of Helsinki principles.

Synthesis and stability of peptides

The RL-QN15 peptide, reduced linear peptide of RL-QN15 without disulfide bonds ($Re_{RL\text{-}QN15}$), linear octapeptide in front of RL-QN15 disulfide bonds ($Li_{RL\text{-}QN15}$), and cyclic heptapeptide composed of an RL-QN15 disulfide-bonded circular structure ($Cy_{RL\text{-}QN15}$) (purity > 95%) were commercially synthesized by Bioyeargene Biotechnology Co., Ltd. (Wuhan, China). The structure of $Cy_{RL\text{-}QN15}$ was predicted using PEP-FOLD3 online service[9]. The stability of RL-QN15 and $Cy_{RL\text{-}QN15}$ was evaluated according to previous research[24].

Cell culture

Human keratinocytes (HaCaT cells), human skin fibroblasts (HSFs), human umbilical vein endothelial cells (HUVECs), and mouse macrophages (RAW 264.7 cells) were cultured in Dulbecco's Modified Eagle Medium (DMEM)/high glucose medium (BI, Israel) supplemented with 1% double antibodies (penicillin and streptomycin) and 10% fetal bovine serum (FBS, Gibco) at 37 °C in a humidified atmosphere of 5% CO_2.

Keratinocyte scratch healing assay

The pro-healing effects of $Cy_{RL\text{-}QN15}$ on HaCaT cells were evaluated according to a previous study[25]. Specific

experimental methods are detailed in section S2.2 of the Supplementary Information.

Effects of RL-QN15-modified peptides on full-thickness skin wounds in mice

The healing effects of $Cy_{RL\text{-}QN15}$ on full-thickness skin wounds in mice were examined according to a previous study[10]. Specific experimental methods are detailed in section S2.3 of the Supplementary Information.

Preparation and characterization of $HPDAlCy_{RL\text{-}QN15}$/ZA hydrogel

Specific experimental methods for the preparation and characterization of the $HPDAlCy_{RL\text{-}QN15}$/ZA hydrogel are detailed in section S2.4 of the Supplementary Information.

Loading and release of $HPDAlCy_{RL\text{-}QN15}$/ZA hydrogel against $Cy_{RL\text{-}QN15}$

The loading efficiency of HPDA and hydrogel against $Cy_{RL\text{-}QN15}$ and the release efficiency of the $HPDAlCy_{RL\text{-}QN15}$/ZA hydrogel against $Cy_{RL\text{-}QN15}$ were determined according a previous study[19].

Biocompatibility and degradation of the $HPDAlCy_{RL\text{-}QN15}$/ZA hydrogel

The toxicity of the $HPDAlCy_{RL\text{-}QN15}$/ZA hydrogel was evaluated in C57BL/6 mice with full-thickness skin wounds and HaCaT cells using the live/dead cell viability assay according to a previous study[19]. The degradation of ZA, HPDA/ZA, $Cy_{RL\text{-}QN15}$/ZA, and $HPDAlCy_{RL\text{-}QN15}$/ZA in vitro and in vivo was determined according to previous studies[26,27]. Specific experimental methods are detailed in section S2.5 of the Supplementary Information.

Assessment of cell proliferation

Cell proliferation was determined using the 3-(4,5-dimethylthiazol-2-yl)-5-(3-carboxymethoxyphenyl)-2-(4-sulfophenyl)-2H-tetrazolium (MTS) assay according to previous methods[19]. Specific experimental methods are detailed in section S2.6 of the Supplementary Information.

In vitro HUVEC migration and tube formation assays

Angiogenesis experiments were performed in vitro according to a previous study[28]. Specific experimental methods are detailed in section S2.7 of the Supplementary Information.

Influence of samples on cytokine levels involved in healing

RAW 264.7 cells (2×10^4 cells/well) were cultured in 6-well plates and incubated with lipopolysaccharide (LPS), vehicle (phosphate-buffered saline, PBS), $Cy_{RL\text{-}QN15}$, $HPDAlCy_{RL\text{-}QN15}$, or $HPDAlCy_{RL\text{-}QN15}$/ZA for 24 h based on previous research[19]. The supernatants were collected to detect the effects on the release of cytokines (transforming growth factor-β1, TGF-β1; tumor necrosis factor-α, TNF-α) using enzyme-linked immunosorbent assay (ELISA) kits (NeoBioscience, Shanghai, China).

Antioxidant activity of the $HPDAlCy_{RL\text{-}QN15}$/ZA hydrogel

The antioxidant activity of the $HPDAlCy_{RL\text{-}QN15}$/ZA hydrogel was evaluated based on free radical scavenging ability and reduction of intracellular reactive oxygen species (ROS). Specific experimental methods are detailed in Section S2.8 of the Supplementary Information.

Effects of samples on chronic diabetic skin wounds in mice

To evaluate the wound healing effects of the $HPDAlCy_{RL\text{-}QN15}$/ZA hydrogel, chronic full-thickness skin wounds in diabetic mice were established according to an earlier study[10]. Specific experimental methods are detailed in Section S2.9 of the Supplementary Information.

Effects of the $HPDAlCy_{RL\text{-}QN15}$/ZA hydrogel on cytokine secretion in skin wounds

Specimens were acquired from the central area of full-thickness skin wounds in diabetic mice on Days 3, 7, and 14 postoperation, homogenized in ice-cold saline (weight/volume = 1:9) at 4 °C and centrifuged at $12000 \times g$ for 20 min at 4 °C to collect the supernatant. The levels of TNF-α and TGF-β1 were detected using ELISA kits (NeoBioscience, Shanghai, China).

Histological analysis and immunohistochemical and immunofluorescence staining

To investigate tissue regeneration, including macrophage polarization (F4/80; inducible nitric oxide synthase, INOS; arginase, ARG), keratinocyte proliferation (Ki67), deposition of collagen (collagen type I, COL I; collagen type III, COL III), angiogenesis (vascular endothelial growth factor, VEGF; α-smooth muscle actin, α-SMA; platelet endothelial cell adhesion molecule, CD31) and the expression of inflammatory factors (interleukin-1β, IL-1β; interleukin-10, IL-10) in skin wounds after different treatments, wound tissues underwent hematoxylin and eosin (H&E), Masson trichrome, periodic acid-Schiff (PAS), and immunohistochemical staining and immunofluorescence analysis according to a previous study[29]. Specific experimental methods are detailed in section S2.10 of the Supplementary Information.

Human ex vivo diabetic skin wound model

The pro-tissue regenerative activity of the $HPDAlCy_{RL\text{-}QN15}$/ZA hydrogel was examined using a modified human skin wound healing assay[30–32]. Specific experimental methods are detailed in section S2.11 of the Supplementary Information.

Results and discussion

The RL-QN15-optimized cyclic heptapeptide $Cy_{RL\text{-}QN15}$ promoted keratinocyte scratch repair and full-thickness skin wound healing in mice

Structural optimization of existing bioactive peptides is important for the development of novel drugs. We previously revealed that the bioactive peptide RL-QN15 exhibits considerable therapeutic effects on skin wounds[10]. As shown in Fig. 1A, RL-QN15 consists of 15 amino acid residues and contains a pair of intramolecular disulfide bonds. Disulfide bonds are critical to the function of amphibian-derived bioactive peptides[10,33,34]. To optimize RL-QN15 and obtain peptides with shorter amino acid sequences and stronger activities, we synthesized $Re_{RL\text{-}QN15}$, $Li_{RL\text{-}QN15}$, and $Cy_{RL\text{-}QN15}$ (Fig. 1A). As shown in Fig. 1B, $Cy_{RL\text{-}QN15}$ contains seven amino acids and links two-terminal cysteine residues to form a closed-loop structure. The predicted structure of $Cy_{RL\text{-}QN15}$ also demonstrated a closed-loop structure (Fig. 1C).

At a concentration of 1 nM, $Li_{RL\text{-}QN15}$ and $Re_{RL\text{-}QN15}$ did not promote HaCaT cell scratch repair, whereas $Cy_{RL\text{-}QN15}$ exhibited similar HaCaT cell scratch pro-healing effects as RL-QN15 (Fig. 1D). The cell scratch repair rates of $Re_{RL\text{-}QN15}$, $Li_{RL\text{-}QN15}$, RL-QN15, and $Cy_{RL\text{-}QN15}$ were 55.1%, 60.8%, 88.1%, and 90.5%, respectively (Fig. 1E).

The therapeutic effects of $Cy_{RL\text{-}QN15}$ on full-thickness skin wounds in mice were explored (Fig. 1F). At a concentration of 1 nM, the wound healing rates of RL-QN15 and $Cy_{RL\text{-}QN15}$ conditions were 91.8% and 94.0%, respectively, higher than those of the positive control rh-bFGF (87.7%) and the $Re_{RL\text{-}QN15}$ (60.0%) and $Li_{RL\text{-}QN15}$ (63.1%) conditions (Fig. 1G). Peptide stability is critical in skin wound treatment, and therefore, we examined the stability of $Cy_{RL\text{-}QN15}$ in plasma. The half-life of $Cy_{RL\text{-}QN15}$ in plasma was 8.07 h, longer than that

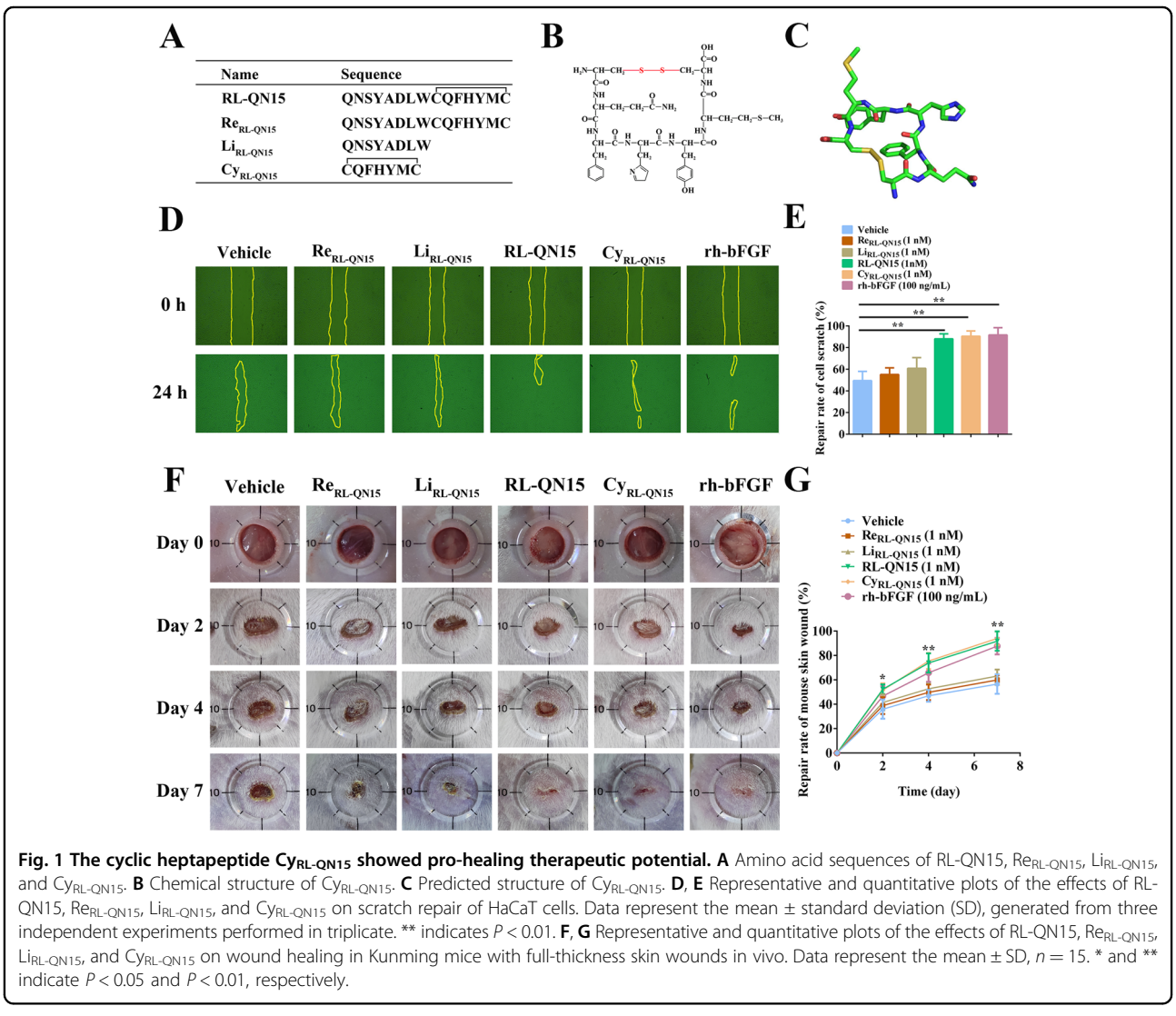

Fig. 1 The cyclic heptapeptide $Cy_{RL\text{-}QN15}$ showed pro-healing therapeutic potential. A Amino acid sequences of RL-QN15, $Re_{RL\text{-}QN15}$, $Li_{RL\text{-}QN15}$, and $Cy_{RL\text{-}QN15}$. **B** Chemical structure of $Cy_{RL\text{-}QN15}$. **C** Predicted structure of $Cy_{RL\text{-}QN15}$. **D**, **E** Representative and quantitative plots of the effects of RL-QN15, $Re_{RL\text{-}QN15}$, $Li_{RL\text{-}QN15}$, and $Cy_{RL\text{-}QN15}$ on scratch repair of HaCaT cells. Data represent the mean ± standard deviation (SD), generated from three independent experiments performed in triplicate. ** indicates $P < 0.01$. **F**, **G** Representative and quantitative plots of the effects of RL-QN15, $Re_{RL\text{-}QN15}$, $Li_{RL\text{-}QN15}$, and $Cy_{RL\text{-}QN15}$ on wound healing in Kunming mice with full-thickness skin wounds in vivo. Data represent the mean ± SD, $n = 15$. * and ** indicate $P < 0.05$ and $P < 0.01$, respectively.

of RL-QN15 (7.79 h), indicating greater stability (Fig. S1A, B). Thus, $Cy_{RL\text{-}QN15}$ exhibited pro-trauma repair activity comparable to that of RL-QN15 but had better stability and lower synthesis costs than RL-QN15, suggesting that it may be a better pro-healing drug candidate.

Characterization and properties of the HPDAlCy$_{RL\text{-}QN15}$/ZA hydrogel

In the current study, we prepared HPDAlCy$_{RL\text{-}QN15}$/ZA hydrogel containing HPDA nanoparticles loaded with $Cy_{RL\text{-}QN15}$ for skin wound healing. As shown in Fig. S2, Zn^{2+} promoted the formation of ZA and HPDAlCy$_{RL\text{-}QN15}$/ZA hydrogels with greater cross-linking than the SA hydrogel. Transmission electron microscopy (TEM) revealed that the HPDA nanoparticles loaded with $Cy_{RL\text{-}QN15}$ had an average grain size of approximately 50 nm, with a spherical morphology and hollow structure, indicating excellent loading capacity (Fig. S3A, B). The morphology and structure of ZA and HPDAlCy$_{RL\text{-}QN15}$/ZA hydrogels were characterized by scanning electron microscopy (SEM), showing a 3D network of microporous structures, which form the basis of the moisture retention and swelling of gels (Fig. 2A, B). Due to the ability of HPDAlCy$_{RL\text{-}QN15}$ to interact with the internal molecules of the ZA hydrogel, the HPDAlCy$_{RL\text{-}QN15}$/ZA hydrogel showed an increased cross-linking density and a denser surface, with a much lower porosity (48.52 ± 0.40%) compared to the ZA hydrogel (56.78 ± 0.10%) (Fig. 2C).

The four Fourier transform infrared (FTIR) spectral curves of the crystal structures of SA, ZA, HPDAlCy$_{RL\text{-}QN15}$, and HPDAlCy$_{RL\text{-}QN15}$/ZA were shown in Fig. 2D. The peak at 3384 cm^{-1} in the SA curve corresponded to the stretching vibration of O-H, which shifted to 3380 cm^{-1} and 3344 cm^{-1} with the formation of ZA and HPDAlCy$_{RL\text{-}QN15}$/ZA hydrogels, respectively. The shift in the HPDAlCy$_{RL\text{-}QN15}$/ZA hydrogel toward lower stretching energy may be related to the presence of imine, amine, catechol, and other groups in HPDA that cause stretching vibrations of the -OH group (Fig. 2D). In addition, the characteristic peak of the -COO stretching vibration at 1610 cm^{-1} in SA shifted to 1607 and 1599 cm^{-1} in the ZA and HPDAlCy$_{RL\text{-}QN15}$/ZA hydrogels, respectively (Fig. 2D). After HPDAlCy$_{RL\text{-}QN15}$ was embedded in the HPDAlCy$_{RL\text{-}QN15}$/ZA hydrogel, the characteristic peak of 1220 cm^{-1} for HPDAlCy$_{RL\text{-}QN15}$ shifted to 1226 cm^{-1} due to the intermolecular interaction between $Cy_{RL\text{-}QN15}$ and alginate, while the SA and ZA hydrogels remained at 1215 cm^{-1}, indicating successful introduction of $Cy_{RL\text{-}QN15}$ into the HPDAlCy$_{RL\text{-}QN15}$/ZA hydrogel (Fig. 2D). The X-ray photoelectron spectroscopy (XPS) spectra of SA, ZA, HPDAlCy$_{RL\text{-}QN15}$, and HPDAlCy$_{RL\text{-}QN15}$/ZA were shown in Fig. 2E. Notably, Na1s, Zn2p, O1s, N1s, C1s, and S2p signal peaks were detected in the HPPDAlCy$_{RL\text{-}QN15}$/ZA hydrogel, indicating the presence of SA, Zn^{2+}, and cyclic peptides with disulfide bonds in the composite. Thus, based on these results, the multifunctional HPDAlCy$_{RL\text{-}QN15}$/ZA hydrogel containing HPDA, $Cy_{RL\text{-}QN15}$, and Zn^{2+} was successfully prepared.

A decreased cross-linking density of the hydrogel results in higher swelling properties[35]. As seen in Fig. 2F, the ZA hydrogel showed excellent swelling properties, while the HPDAlCy$_{RL\text{-}QN15}$/ZA hydrogel showed a lower swelling ratio. The lower swelling ratio of the HPDAlCy$_{RL\text{-}QN15}$/ZA hydrogel may be related to HPDAlCy$_{RL\text{-}QN15}$ interacting with the internal molecules of the ZA hydrogel and increasing its cross-linking density, consistent with the SEM and porosity results. The mechanical properties of hydrogels applied to wounds or tissue engineering are crucial[36]; thus, we determined the rheological and compression properties of the hydrogels. The rheological properties of storage modulus (G') and loss modulus (G") of ZA, HPDA/ZA, Cy$_{RL\text{-}QN15}$/ZA, and HPDAlCy$_{RL\text{-}QN15}$/ZA hydrogels were measured in the frequency range of 0–10 Hz at 37 °C. The results showed that G' was greater than G" for all groups, with the HPDAlCy$_{RL\text{-}QN15}$/ZA hydrogel showing the most significant difference, indicating greater flexibility (Fig. S4A). The G' and G" values of the HPDAlCy$_{RL\text{-}QN15}$/ZA hydrogel did not change with increasing oscillation frequency, indicating that the HPDAlCy$_{RL\text{-}QN15}$/ZA hydrogel has excellent stability (Fig. S4A). The compression properties of the HPDAlCy$_{RL\text{-}QN15}$/ZA hydrogel were enhanced by the cross-linking of Zn^{2+} and the internal molecular interactions between HPDAlCy$_{RL\text{-}QN15}$ and ZA, demonstrating higher compressive strength (more than 250 kPa to 80% strain) than the ZA, HPDA/ZA, and Cy$_{RL\text{-}QN15}$/ZA hydrogels (Fig. S4B).

The loading of $Cy_{RL\text{-}QN15}$ and its slow-release from Cy$_{RL\text{-}QN15}$/ZA, HPDAlCy$_{RL\text{-}QN15}$, and HPDAlCy$_{RL\text{-}QN15}$/ZA were evaluated. As shown in Fig. 2G, the loading efficiencies of HPDAlCy$_{RL\text{-}QN15}$/ZA, HPDAlCy$_{RL\text{-}QN15}$, and Cy$_{RL\text{-}QN15}$/ZA against $Cy_{RL\text{-}QN15}$ were 44.61, 50.62, and 87.86%, respectively. When dispersed in PBS, HPDAlCy$_{RL\text{-}QN15}$, Cy$_{RL\text{-}QN15}$/ZA, and HPDAlCy$_{RL\text{-}QN15}$/ZA released $Cy_{RL\text{-}QN15}$ into the solvent in a sustained manner (Fig. 2H). As shown in Fig. 2H, the efficiency of $Cy_{RL\text{-}QN15}$ release from Cy$_{RL\text{-}QN15}$/ZA, HPDAlCy$_{RL\text{-}QN15}$, and HPDAlCy$_{RL\text{-}QN15}$/ZA sequentially decreased, with release rates of >50% at 24 h, reaching 93.51, 79.89, and 73.48% at 48 h, respectively. The sustained-release of $Cy_{RL\text{-}QN15}$ by the HPDAlCy$_{RL\text{-}QN15}$/ZA hydrogel prolonged the effects of the peptide, and the release rates of $Cy_{RL\text{-}QN15}$ peaked at 48 h, thus exerting effects on the inflammatory and proliferative phases of wound repair. In summary, we successfully prepared the HPDAlCy$_{RL\text{-}QN15}$/ZA hydrogel with excellent mechanical properties and $Cy_{RL\text{-}QN15}$ loading and slow-release properties.

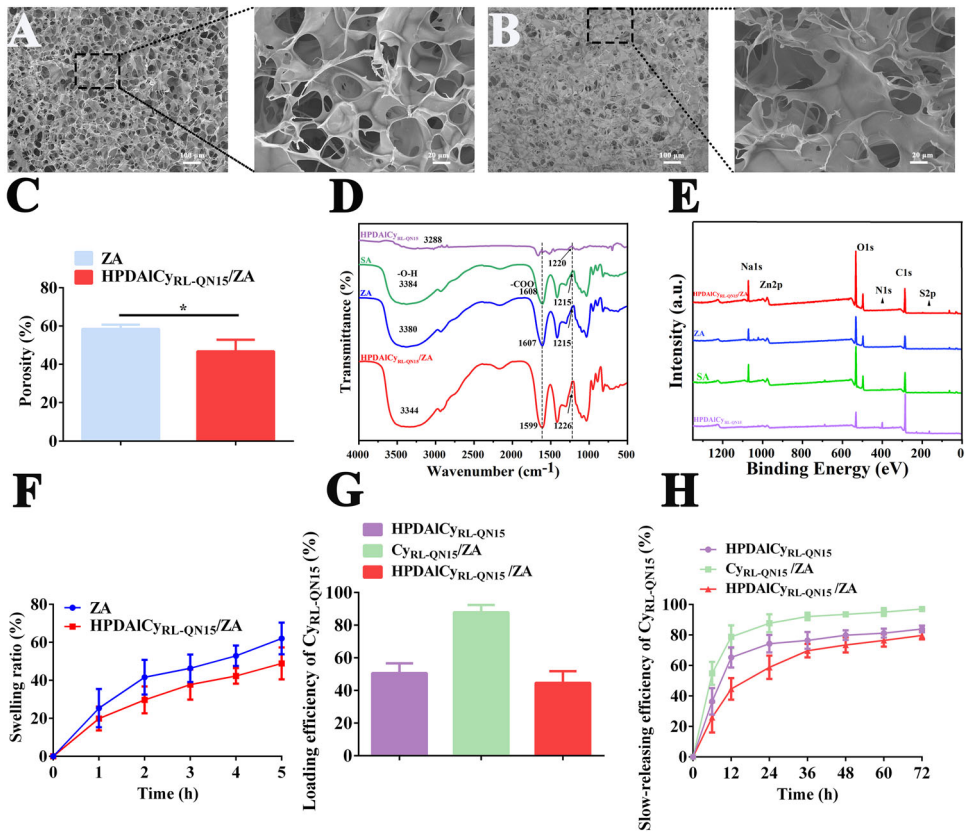

Fig. 2 Characterization and properties of the HPDAlCy$_{RL-QN15}$/ZA hydrogel. A, **B** SEM images of the ZA and HPDAlCy$_{RL-QN15}$/ZA hydrogels, respectively. The scale (100 μm and 20 μm) is represented by the line in the lower left corner of the figure. **C** Porosity of the ZA and HPDAlCy$_{RL-QN15}$/ZA hydrogels. Data represent the mean ± SD, generated from three independent experiments. * indicates $P < 0.05$. **D**, **E** FTIR and XPS analyses of the SA, ZA, HPDAlCy$_{RL-QN15}$, and HPDAlCy$_{RL-QN15}$/ZA, respectively. **F** Swelling ratio of the ZA and HPDAlCy$_{RL-QN15}$/ZA hydrogels. **G**, **H** Loading efficiency of Cy$_{RL-QN15}$ and the efficiency of its slow-release from the HPDAlCy$_{RL-QN15}$, Cy$_{RL-QN15}$/ZA, and HPDAlCy$_{RL-QN15}$/ZA. Data represent the mean ± SD, generated from three independent experiments performed in triplicate.

Biocompatibility and degradation of the HPDAlCy$_{RL-QN15}$/ZA hydrogel

Biocompatibility is an important property regarding the potential safety of novel biomaterials[37]. As shown in Fig. S5A, nearly all HaCaT cells were stained with calcein-AM ester (green fluorescence), with very few dead cells stained with PI (red fluorescence), indicating that ZA, HPDA, Cy$_{RL-QN15}$, HPDA/ZA, Cy$_{RL-QN15}$/ZA, HPDAlCy$_{RL-QN15}$, and HPDAlCy$_{RL-QN15}$/ZA exhibited no toxicity toward HaCaT cells. The C57BL/6 mouse dorsal skin wound toxicity assay also revealed that ZA, HPDA, Cy$_{RL-QN15}$, HPDA/ZA, Cy$_{RL-QN15}$/ZA, HPDAlCy$_{RL-QN15}$, and HPDAlCy$_{RL-QN15}$/ZA caused no mortality in mice, and histological sections of major organs (heart, liver, spleen, lung, and kidney) from treated mice showed no abnormalities (Fig. S5B). The degradation of hydrogels in vivo is also crucial for their application in skin wound healing[38]. Thus, we evaluated the degradation of hydrogels in vitro and in vivo (Fig. S6). The results showed that the hydrogels gradually decreased in size with increasing incubation time under hyaluronidase and collagenase treatment; after 120 h of treatment, the remaining amounts of ZA, HPDA/ZA, Cy$_{RL-QN15}$/ZA, and HPDAlCy$_{RL-QN15}$/ZA hydrogels were 19.8, 23.2, 23.4, and 29.8%, respectively (Fig. S6A). The ZA, HPDA/ZA, Cy$_{RL-QN15}$/ZA, and HPDAlCy$_{RL-QN15}$/ZA hydrogels also showed great degradation efficacy when injected subcutaneously into the abdomens of mice, with all hydrogels fully degrading two weeks after injection (Fig. S6B). In conclusion, the HPDAlCy$_{RL-QN15}$/ZA hydrogel showed negligible cytotoxicity, excellent biocompatibility, and excellent degradation properties, providing a foundation for its pro-healing therapeutic potential in skin wounds.

HPDAlCy$_{RL-QN15}$/ZA hydrogel promoted cell proliferation and scratching healing

The MTS results showed that ZA, HPDA/ZA, Cy$_{RL-QN15}$, HPDAlCy$_{RL-QN15}$, and HPDAlCy$_{RL-QN15}$/ZA exhibited significantly proliferation-promoting activity toward HaCaT cells, HSFs, and HUVECs (Fig. 3A–C) but did not

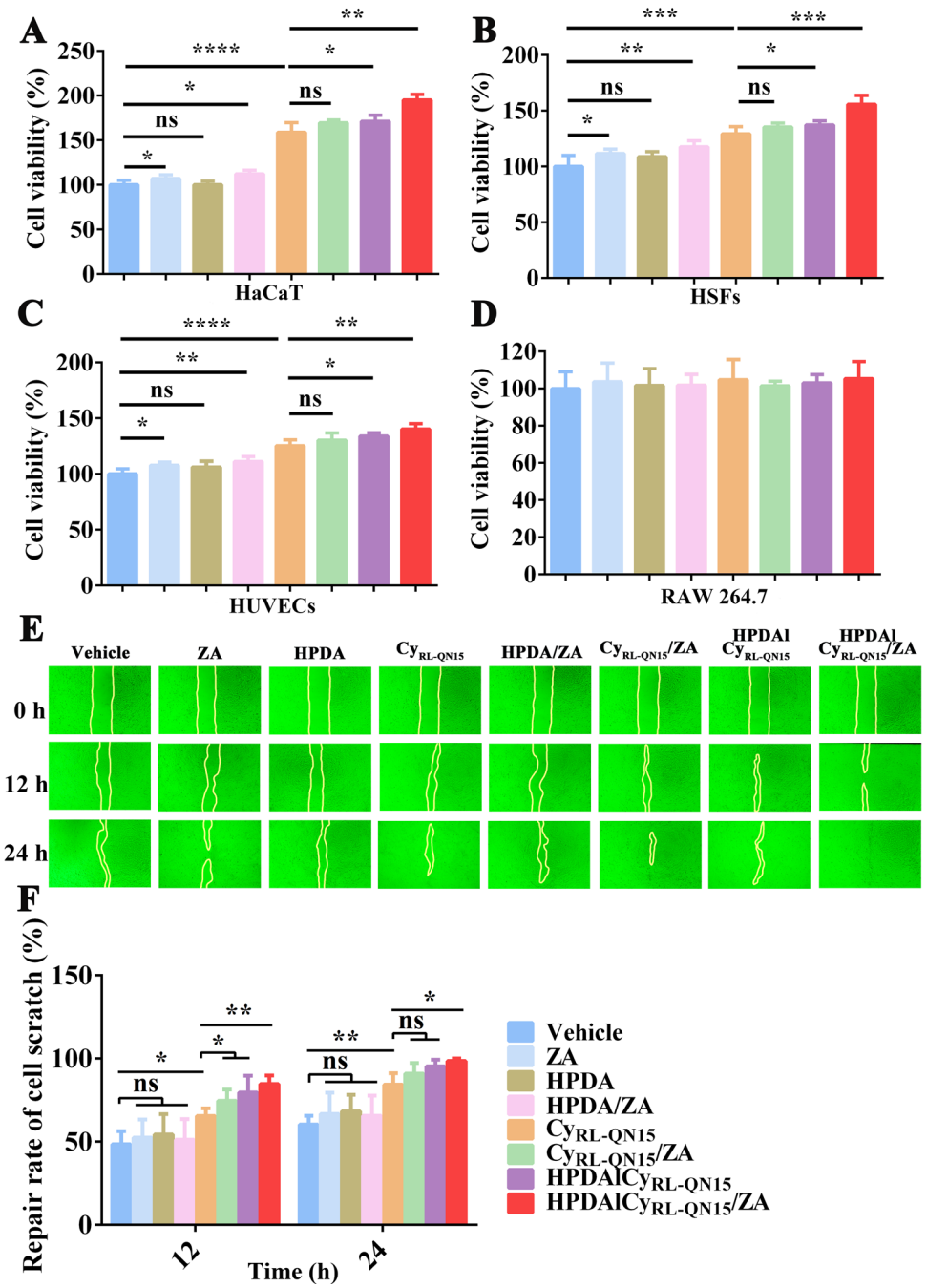

Fig. 3 The HPDAlCy$_{RL\text{-}QN15}$/ZA hydrogel promoted cell proliferation and scratch healing. A–D Effects of vehicle (PBS), ZA, HPDA nanoparticles, HPDA/ZA, Cy$_{RL\text{-}QN15}$, Cy$_{RL\text{-}QN15}$/ZA, HPDAlCy$_{RL\text{-}QN15}$, and HPDAlCy$_{RL\text{-}QN15}$/ZA conditions on the proliferation of HaCaT cells, HSFs, HUVECs, and RAW 264.7 cells. Data represent the mean ± SD, generated from three independent experiments performed in triplicate. *, **, ***, and **** indicate $P < 0.05$, $P < 0.01$, $P < 0.001$, and $P < 0.0001$, respectively. **E** Representative images showing the pro-healing effects of the samples against HaCaT cell scratches. **F** Quantification of the pro-healing effects of the samples against HaCaT cell scratches. Data represent the mean ± SD, generated from three independent experiments performed in triplicate. * and ** indicate $P < 0.05$ and $P < 0.01$, respectively.

affect the proliferation of macrophages (Fig. 3D). The HPDAlCy$_{RL\text{-}QN15}$/ZA hydrogel showed the most significant cell pro-proliferation effect, indicating that the multi-functional HPDAlCy$_{RL\text{-}QN15}$/ZA hydrogel, incorporating Zn^{2+}, HPDA, and ZA, greatly enhanced the cell proliferation-promoting activity of Cy$_{RL\text{-}QN15}$.

The cell wound pro-healing potential of the HPDAl-Cy$_{RL\text{-}QN15}$/ZA hydrogel was demonstrated using a

keratinocyte scratch assay (Fig. 3E). Compared to the vehicle (52.02 ± 4.02%), ZA and HPDA/ZA showed no obvious pro-healing effects, while $Cy_{RL\text{-}QN15}$, $Cy_{RL\text{-}QN15}$/ZA, $HPDAlCy_{RL\text{-}QN15}$, and $HPDAlCy_{RL\text{-}QN15}$/ZA showed great pro-healing activity, with scratch repair rates of 89.51 ± 3.88, 90.84 ± 2.75, 92.83 ± 2.75, and 95.23 ± 4.49%, respectively (Fig. 3F). $Cy_{RL\text{-}QN15}$ exhibited excellent scratch healing activity, and its scratch healing activity was significantly enhanced by $HPDAlCy_{RL\text{-}QN15}$ and $HPDAlCy_{RL\text{-}QN15}$/ZA.

The $HPDAlCy_{RL\text{-}QN15}$/ZA hydrogel regulated the release of cytokines from macrophages, promoted angiogenesis, and exerted antioxidant activities

Macrophages play a pivotal role in wound healing, particularly in the secretion of cytokines and inflammatory factors that regulate the wound repair process, thereby facilitating skin wound healing[39]. $Cy_{RL\text{-}QN15}$ significantly decreased the expression of TNF-α induced by LPS but promoted the expression of TGF-β1. More importantly, the $HPDAlCy_{RL\text{-}QN15}$ and $HPDAlCy_{RL\text{-}QN15}$/ZA enhanced the regulatory activity of $Cy_{RL\text{-}QN15}$ on cytokine release from macrophages (Fig. 4A, B). The $HPDAlCy_{RL\text{-}QN15}$/ZA hydrogel exerted the best effects, reducing the expression of TNF-α from 850.89 ± 75.25 pg/mL (LPS) to 674.83 ± 34.48 pg/mL while promoting the expression of TGF-β1 from 99.45 ± 20.96 pg/mL (vehicle) to 315.50 ± 63.50 pg/mL (Fig. 4A, B).

The effects of the $HPDAlCy_{RL\text{-}QN15}$/ZA hydrogel on HUVEC migration and tube formation were explored (Fig. 4C, D). Compared to the vehicle, $Cy_{RL\text{-}QN15}$ significantly promoted HUVEC migration (by 1.23-fold), while the $HPDAlCy_{RL\text{-}QN15}$ and $HPDAlCy_{RL\text{-}QN15}$/ZA significantly enhanced the cell pro-migration activity of $Cy_{RL\text{-}QN15}$ (by 1.42- and 1.58-fold, respectively) (Fig. 4E). After treatment with $Cy_{RL\text{-}QN15}$, $HPDAlCy_{RL\text{-}QN15}$, and $HPDAlCy_{RL\text{-}QN15}$/ZA, HUVEC tube formation reached 231 ± 26.94, 286.33 ± 6.01, and 347.33 ± 14.19, respectively (Fig. 4F). These results indicate that the $HPDAlCy_{RL\text{-}QN15}$/ZA hydrogel significantly enhanced the activity of $Cy_{RL\text{-}QN15}$, especially by its loading and slow release from HPDA, as well as the pro-proliferative and angiogenic activities of Zn^{2+}.

Excessive production of ROS in the wound area can cause oxidative stress, leading to cellular DNA damage and impaired angiogenesis; therefore, removal of excessive ROS effectively promotes wound healing[40,41]. $Cy_{RL\text{-}QN15}$ showed no free radical scavenging capacity, whereas HPDA exhibited free radical scavenging and ROS reducing activities; therefore, both $HPDAlCy_{RL\text{-}QN15}$ and $HPDAlCy_{RL\text{-}QN15}$/ZA exhibited free radical scavenging and ROS reducing activities (Fig. S7). As seen in Fig. S7A, B, the $HPDAlCy_{RL\text{-}QN15}$/ZA hydrogel showed direct scavenging activity against 2, 2'-azino-bis (3-ethylbenzothiazoline-6-sulfonic acid) ($ABTS^{+}$) (53.01 ± 2.84%) and 2,2-diphenyl-1-picrylhydrazyl (DPPH free radicals) (42.06 ± 2.89%), with similar activity as the positive control vitamin C (VC). The intracellular scavenging ability of the $HPDAlCy_{RL\text{-}QN15}$/ZA hydrogel against ROS in HUVECs stimulated with hydrogen peroxide (H_2O_2) was also assessed by flow cytometry. ROS intensity increased significantly (4123.66 ± 415.54) following H_2O_2 stimulation but decreased significantly under $HPDAlCy_{RL\text{-}QN15}$ and $HPDAlCy_{RL\text{-}QN15}$/ZA treatment (2795 ± 214.41 and 2285.66 ± 134.50, respectively) (Fig. S7C, D). In conclusion, the multifunctional $HPDAlCy_{RL\text{-}QN15}$/ZA hydrogel not only exhibited regulatory effects on cytokine release in macrophages but also promoted HUVEC migration and free radical scavenging and reduced excessive ROS in HUVECs. Thus, this hydrogel shows excellent therapeutic potential for the treatment of chronic skin injuries, such as diabetic wounds.

The $HPDAlCy_{RL\text{-}QN15}$/ZA hydrogel promoted full-thickness wound healing, epidermal regeneration, and collagen deposition in diabetic mice

The application of multifunctional hydrogel dressings with anti-inflammatory, antioxidant, and angiogenic activities provides a new strategy for skin wound treatment, especially chronic wound healing[42]. With its superior biocompatibility, the multifunctional $HPDAlCy_{RL\text{-}QN15}$/ZA hydrogel showed excellent potential for the treatment of chronic skin wounds (Figs. 3, 4, S5, and S7). Thus, we further investigated its pro-healing activity on diabetic skin wounds in mice. Wounds in type 2 diabetic mice were treated with the different compounds and then monitored at different times to determine the change in wound area (Fig. 5A). The results showed that the repairing effect of $Cy_{RL\text{-}QN15}$ on wounds was significantly better than that of the vehicle or commercial dressing (Tegaderm), and the $HPDAlCy_{RL\text{-}QN15}$/ZA hydrogel significantly enhanced the skin regenerative effects of $Cy_{RL\text{-}QN15}$. Notably, after 14 days of treatment, the $HPDAlCy_{RL\text{-}QN15}$/ZA hydrogel-treated wounds were almost completely healed without obvious scarring, while the $Cy_{RL\text{-}QN15}$- and $HPDAlCy_{RL\text{-}QN15}$-treated wounds were mostly healed with a small amount of scabbing. In contrast, the Tegaderm- and vehicle-treated wounds were not healed and showed considerable scarring. On Day 14, compared with the vehicle (66.38 ± 3.41%), the skin tissue repair rates of the $Cy_{RL\text{-}QN15}$, $HPDAlCy_{RL\text{-}QN15}$, and $HPDAlCy_{RL\text{-}QN15}$/ZA were 88.74 ± 2.14, 92.64 ± 2.72, and 95.23 ± 4.49%, respectively, demonstrating that the $HPDAlCy_{RL\text{-}QN15}$/ZA hydrogel exhibited the highest pro-regeneration effects on diabetic skin wounds in mice (Fig. 5B).

H&E staining was performed to evaluate skin wound healing and regeneration on Days 3, 7, and 14 (Fig. 5C–F). From Days 3 to 14, wounds treated with the $HPDAlCy_{RL\text{-}QN15}$/ZA hydrogel exhibited the best regeneration of epidermal integrity and thickness. On Day 14,

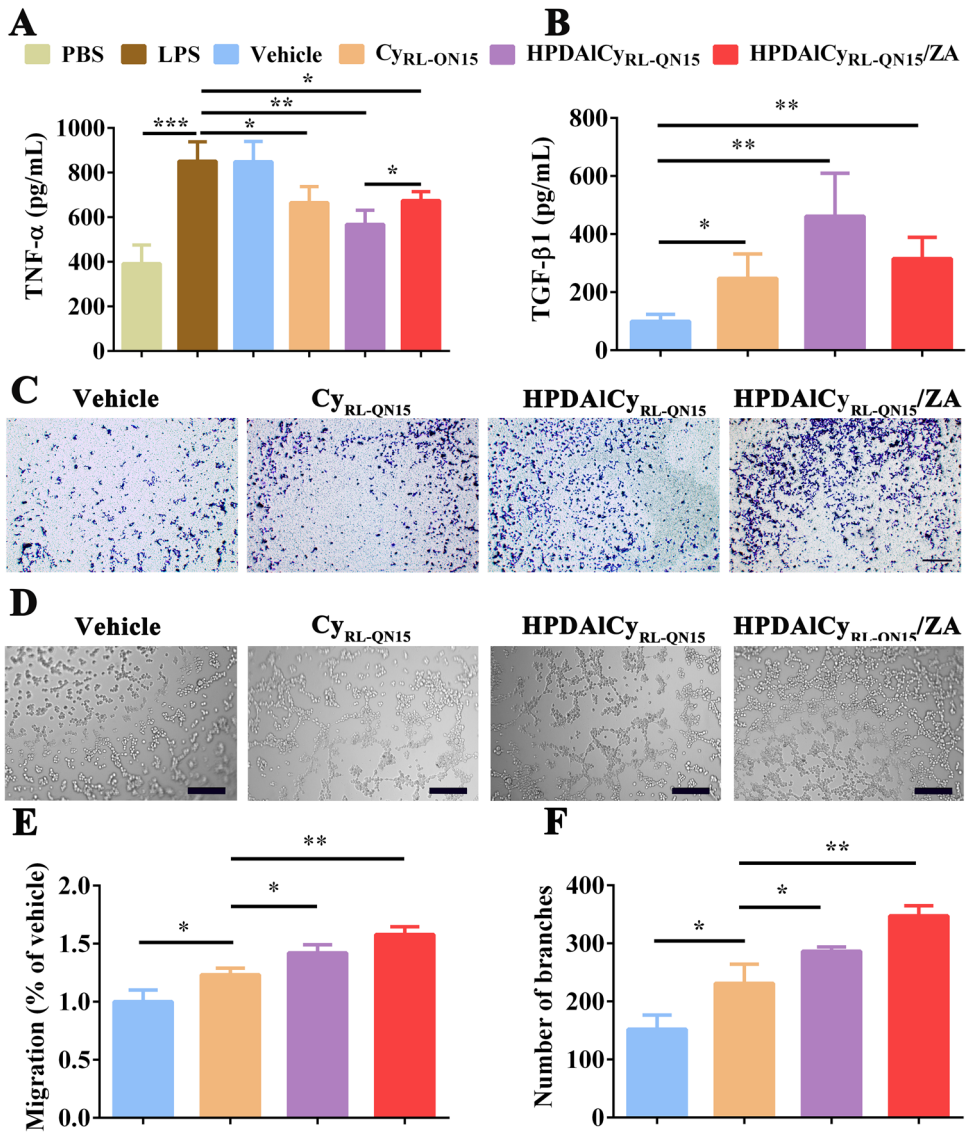

Fig. 4 Effects of the HPDAlCy$_{RL-QN15}$/ZA hydrogel on macrophage cytokine secretion, HUVEC migration, and tube formation. A Effects of vehicle (PBS), Cy$_{RL-QN15}$, HPDAlCy$_{RL-QN15}$, and HPDAlCy$_{RL-QN15}$/ZA conditions on TNF-α release in RAW 264.7 cells stimulated with LPS. **B** Effects of vehicle (PBS), Cy$_{RL-QN15}$, HPDAlCy$_{RL-QN15}$, and HPDAlCy$_{RL-QN15}$/ZA conditions on TGF-β1 release in RAW 264.7 cells. **C**, **E** Representative images showing HUVEC migration and quantitative analysis, respectively. Scale bar: 200 μm. **D**, **F** Representative images of HUVEC tube formation and quantitative analysis, respectively. Scale bar: 200 μm. Data represent the mean ± SD, generated from three independent experiments performed in triplicate. *, **, and *** indicate $P < 0.05$, $P < 0.01$, and $P < 0.001$, respectively.

Cy$_{RL-QN15}$ treatment showed superior neo-epidermal (173 ± 6.23 μm) and granulation tissue thickness (576.33 ± 9.80 μm) in the wound compared to the vehicle and Tegaderm groups. Notably, compared to treatment with Cy$_{RL-QN15}$, wounds treated with the HPDAlCy$_{RL-QN15}$/ZA hydrogel exhibited better therapeutic efficacy, in which neo-epidermal and granulation tissue thicknesses reached 198 ± 5.09 μm and 669 ± 8.64 μm, respectively (Fig. 5D, E). As shown in Fig. S8A, C, compared with the vehicle group (99.95 ± 26.97), immunofluorescence staining of Ki67 in injured tissue on postoperative Day 14 also indicated that the HPDAlCy$_{RL-QN15}$/ZA hydrogel (279.52 ± 25.60) significantly enhanced the expression of the epidermal cell proliferation marker Ki67.

Masson trichrome and PAS staining showed significantly greater collagen deposition and basement membrane completion in the regenerated tissue with HPDAlCy$_{RL-QN15}$/ZA hydrogel treatment (Fig. 5C). As seen in Fig. S8B, D, E, the HPDAlCy$_{RL-QN15}$/ZA hydrogel-treated wounds showed significantly higher positive

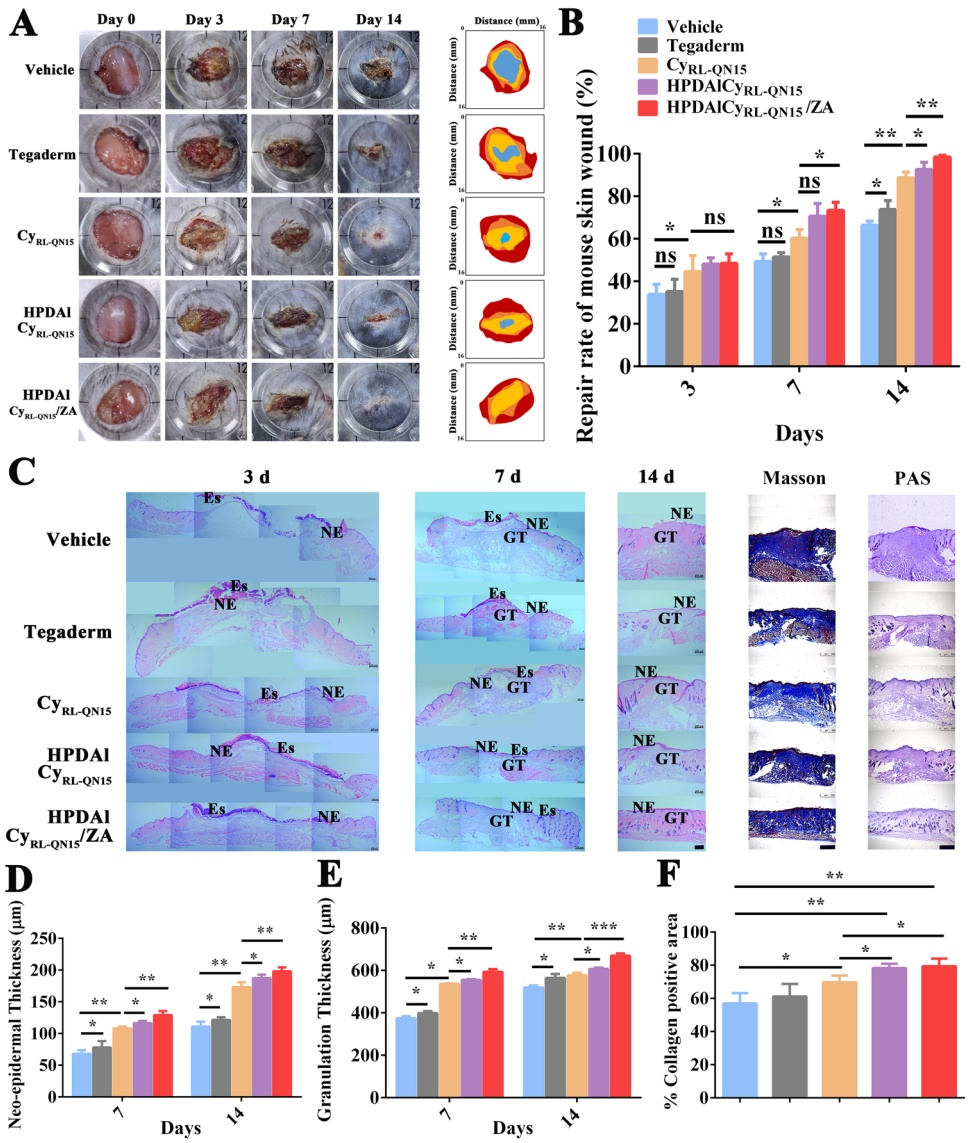

Fig. 5 The HPDAICy$_{RL\text{-}QN15}$/ZA hydrogel promoted the repair and tissue regeneration of full-thickness skin wounds in type 2 diabetic mice. **A** Representative images of wounds in each group during the healing process and schematic of the wound healing process in the five groups. **B** Quantitative data of wound repair rates at different time points in the five groups. **C** Representative H&E staining images of wound specimens from different groups on Days 3, 7, and 14. Masson trichrome and PAS staining on Day 14. Es eschar, NE newborn epithelium, GT granulation tissue. Scale bar: 500 μm. **D**–**F** Quantification of regenerated epidermis thickness, granulation tissue thickness, and collagen deposition in wounds. All data represent the mean ± SD generated from three independent experiments performed in triplicate. *, **, and *** indicate $P < 0.05$, $P < 0.01$, and $P < 0.001$, respectively.

staining intensity for collagen types I and III (COL I and COL III, respectively) compared with the other treatment groups, consistent with its promotion of fibroblast proliferation and collagen deposition. These findings indicated that the HPDAICy$_{RL\text{-}QN15}$/ZA hydrogel enhanced the pro-healing effects of Cy$_{RL\text{-}QN15}$ in chronic skin wounds, resulting in shortened healing time, thicker neoepidermis, superior granulation tissue formation, and greater collagen deposition.

The HPDAICy$_{RL\text{-}QN15}$/ZA hydrogel promoted macrophage polarization (M1 to M2) to reduce inflammation and angiogenesis

Markers of the macrophage M1 (F4/80/INOS) and M2 phenotypes (F4/80/ARG) were stained with immunofluorescence to evaluate the effects of the HPDAICy$_{RL\text{-}QN15}$/ZA hydrogel on macrophage polarization (Fig. 6A, B). Immunofluorescence showed that the positive rate of F4/80/INOS (INOS$^+$/F4/80$^+$) in the vehicle, Tegaderm,

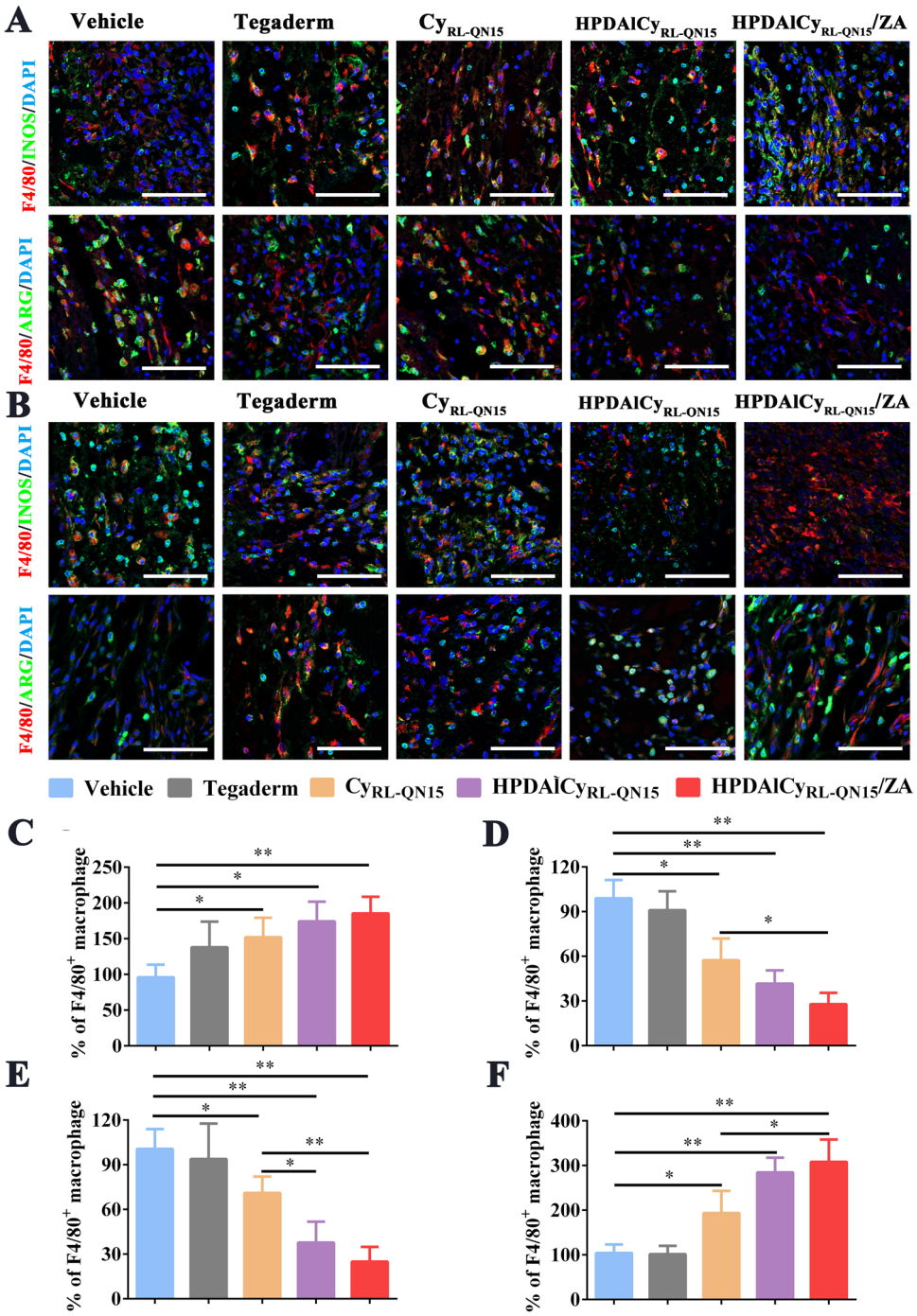

Fig. 6 The HPDAlCy$_{RL-QN15}$/ZA hydrogel alleviated the inflammation of diabetic wounds and stimulated the M2 polarization of macrophages. A Representative images of F4/80, INOS, and ARG staining on Day 3. Scale bar: 50 μm. **B** Representative images of F4/80, INOS, and ARG staining on Day 7. Scale bar: 50 μm. **C**, **D** Ratio of INOS-positive to F4/80-positive macrophages (INOS$^+$/F4/80$^+$) on Days 3 and 7. **E**, **F** Ratio of ARG-positive to F4/80-positive macrophages (ARG$^+$/F4/80$^+$) on Days 3 and 7. Data represent the mean ± SD, generated from three independent experiments performed in triplicate. * and ** indicate $P < 0.05$ and $P < 0.01$, respectively.

Cy$_{RL-QN15}$, HPDAlCy$_{RL-QN15}$, and HPDAlCy$_{RL-QN15}$/ZA groups increased sequentially on Day 3 (95.99 ± 14.42, 138.09 ± 29.11, 152.08 ± 22.16, 174.30 ± 22.43, and 185.29 ± 8.08, respectively) (Fig. 6C). On Day 7, the INOS$^+$/F4/80$^+$ ratio in the different groups decreased sequentially, from 98.96 ± 10.05 in the vehicle group to 57.34 ± 11.89 in the

$Cy_{RL\text{-}QN15}$ group and 27.81 ± 6.22 in the $HPDAlCy_{RL\text{-}QN15}$/ZA hydrogel group (Fig. 6D). On Days 3 and 7, the positive rate of ARG/F4/80 ($ARG^+/F4/80^+$) showed the opposite trend to $INOS^+/F4/80^+$ in $Cy_{RL\text{-}QN15}$, $HPDAlCy_{RL\text{-}QN15}$, and $HPDAlCy_{RL\text{-}QN15}$/ZA, with the greatest increase being seen in the $HPDAlCy_{RL\text{-}QN15}$/ZA hydrogel (from 24.97 ± 8.02 to 308.26 ± 40.72) (Fig. 6E), which indicated the greatest increase in M2 phenotype macrophages in the wound tissue (Fig. 6E, F). These results suggested that $Cy_{RL\text{-}QN15}$ regulated macrophage polarization and the $HPDAlCy_{RL\text{-}QN15}$/ZA hydrogel significantly enhanced $Cy_{RL\text{-}QN15}$ activity.

As shown in Fig. S9A, B, the expression level of TNF-α decreased after $Cy_{RL\text{-}QN15}$, $HPDAlCy_{RL\text{-}QN15}$, and $HPDAlCy_{RL\text{-}QN15}$/ZA treatment, whereas the expression level of TGF-β1 showed the opposite pattern, consistent with the in vitro results. After 7 days of treatment with $Cy_{RL\text{-}QN15}$, $HPDAlCy_{RL\text{-}QN15}$, and $HPDAlCy_{RL\text{-}QN15}$/ZA, the expression levels of IL-1β decreased, while the expression levels of IL-10 increased (Fig. S9C–E). Thus, $Cy_{RL\text{-}QN15}$ promoted macrophage polarization to the M2 phenotype to reduce inflammation, while the $HPDAlCy_{RL\text{-}QN15}$/ZA hydrogel enhanced the regulatory activity of $Cy_{RL\text{-}QN15}$.

As M2 macrophages and Zn^{2+} can promote angiogenesis[18,43] and both $Cy_{RL\text{-}QN15}$ and $HPDAlCy_{RL\text{-}QN15}$/ZA promoted the transformation of macrophages to M2, their effects on angiogenesis were explored by immunofluorescence analysis of VEGF, CD31, and α-SMA in skin wounds. VEGF can promote endothelial cell migration and angiogenesis, CD31 and α-SMA are common markers of angiogenesis, and α-SMA also promotes wound contraction[44]. Compared with the vehicle, the positive staining intensities of VEGF, α-SMA, and CD31 were enhanced after treatment with $Cy_{RL\text{-}QN15}$, $HPDAlCy_{RL\text{-}QN15}$, and $HPDAlCy_{RL\text{-}QN15}$/ZA, indicating promotion of angiogenic activity (Figs. 7A–D, S10A, B). $Cy_{RL\text{-}QN15}$ enhanced the expression of CD31, and $HPDAlCy_{RL\text{-}QN15}$ markedly enhanced the expression levels of VEGF, α-SMA, and CD31 (Figs. 7C, D, S10B). Notably, the $HPDAlCy_{RL\text{-}QN15}$/ZA hydrogel showed the greatest promotion of angiogenesis, increasing the expression levels of VEGF, α-SMA, and CD31 by 3.1-, 2.6-, and 3.3-fold, respectively, compared to the vehicle (Figs. 7C, D, S10B). $Cy_{RL\text{-}QN15}$ significantly promoted angiogenesis in diabetic mouse skin wounds. The $HPDAlCy_{RL\text{-}QN15}$ and $HPDAlCy_{RL\text{-}QN15}$/ZA enhanced $Cy_{RL\text{-}QN15}$ activity, with the $HPDAlCy_{RL\text{-}QN15}$/ZA hydrogel exhibiting the strongest angiogenic activity due to the combination of Zn^{2+} and $Cy_{RL\text{-}QN15}$. In summary, the $HPDAlCy_{RL\text{-}QN15}$/ZA hydrogel markedly enhanced $Cy_{RL\text{-}QN15}$ peptide activity, suppressed the inflammatory response by stimulating macrophage polarization from the M1 to M2 phenotype, and promoted Ki67, VEGF, CD31, α-SMA, COL I, and COL III expression to accelerate epithelialization and facilitate blood vessel regeneration, collagen deposition, and granulation tissue regeneration. Thus, this hydrogel exhibits excellent therapeutic potential in the healing of chronic diabetic skin wounds.

The $HPDAlCy_{RL\text{-}QN15}$/ZA hydrogel boosted skin wound repair in cultured ex vivo diabetic patient skin

The $HPDAlCy_{RL\text{-}QN15}$/ZA hydrogel exhibited similar anti-inflammatory and angiogenesis-promoting properties as the multifunctional GelMA/AA/Cu and PC/GO/Met hydrogels, showing excellent therapeutic effects on chronic diabetic wounds at the animal level[45,46]. In addition, the $HPDAlCy_{RL\text{-}QN15}$/ZA hydrogel also exhibited free radical scavenging and oxidative stress reducing activities, which are essential for the recovery of cellular function in diabetic wound areas (Fig. S7). To better explore the therapeutic effects of the $HPDAlCy_{RL\text{-}QN15}$/ZA hydrogel on skin wounds in diabetic patients, an ex vivo diabetic skin wound healing model was established (Fig. 8A, B). PAS staining showed that the skin in all treatment groups maintained a normal structure, with no epidermal detachment and no significant changes at the dermal-epidermal junction, indicating successful construction of the model (Fig. 8C). Compared with the vehicle (0.56 ± 0.07 mm and 0.29 ± 0.05 mm), the $HPDAlCy_{RL\text{-}QN15}$/ZA hydrogel significantly stimulated re-epithelialization, with a markedly thicker epidermis (0.77 ± 0.07 mm) and epidermal migration (0.5 ± 0.05 mm) from the edge to the center of the wound (Fig. 8D, E). The level of collagen deposition in granulation tissue is a principal marker of wound healing[47]. As shown in Fig. 8F, collagen deposition in the $HPDAlCy_{RL\text{-}QN15}$/ZA hydrogel group (81.62 ± 7.90%) was significantly higher than that in the $HPDAlCy_{RL\text{-}QN15}$ (70.21 ± 5.71%), $Cy_{RL\text{-}QN15}$ (65.86 ± 4.38%), and vehicle groups (58.15 ± 5.00%).

The ELISA results showed that the expression level of TNF-α in the in vitro diabetic skin wounds was significantly lower in the $Cy_{RL\text{-}QN15}$, $HPDAlCy_{RL\text{-}QN15}$, and $HPDAlCy_{RL\text{-}QN15}$/ZA groups than in the vehicle group, while the expression level of TGF-β1 was significantly higher after $HPDAlCy_{RL\text{-}QN15}$ and especially $HPDAlCy_{RL\text{-}QN15}$/ZA treatment (Fig. 8G, H). Immunofluorescence staining of the vascular regeneration-related markers CD31 and α-SMA was performed to detect angiogenesis in ex vivo foot skin wounds of diabetic patients (Fig. S11). As shown in Fig. S11B, D, α-SMA expression in the $Cy_{RL\text{-}QN15}$, $HPDAlCy_{RL\text{-}QN15}$, and $HPDAlCy_{RL\text{-}QN15}$/ZA groups differed insignificantly from that in the vehicle (PBS) group. In contrast, the expression levels of CD31 in the $HPDAlCy_{RL\text{-}QN15}$ and $HPDAlCy_{RL\text{-}QN15}$/ZA groups were 169.60 ± 9.63 and 170.10 ± 10.92%, respectively, significantly higher than that of $Cy_{RL\text{-}QN15}$ (150.32 ± 12.80%) (Fig. S11A, C).

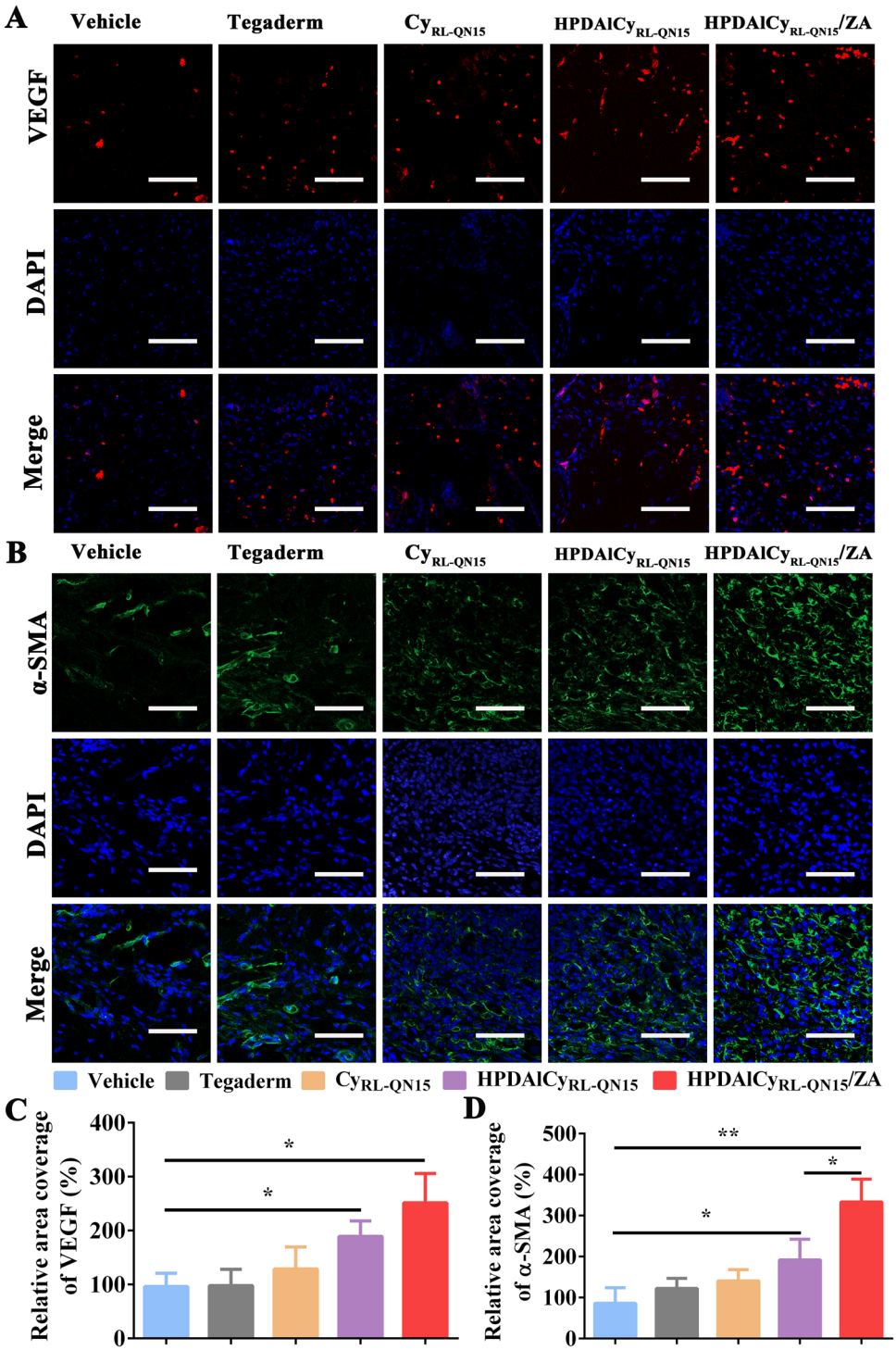

Fig. 7 Effect of the HPDAlCy$_{RL-QN15}$/ZA hydrogel on angiogenesis. A, **B** Representative images of immunofluorescence staining of VEGF and α-SMA in diabetic mice on Day 14 after treatment. Scale bar: 50 μm. **C**, **D** Quantitative data of VEGF and α-SMA in wounds, respectively. Data represent the mean ± SD, generated from three independent experiments performed in triplicate. * and ** indicate $P < 0.05$ and $P < 0.01$, respectively.

These results demonstrated that the HPDAlCy$_{RL-QN15}$/ZA hydrogel inhibited inflammation, promoted re-epithelialization, and accelerated angiogenesis, thus exhibiting excellent therapeutic effects on ex vivo diabetic patient skin wounds and providing a new strategy and candidate for the treatment of chronic wounds.

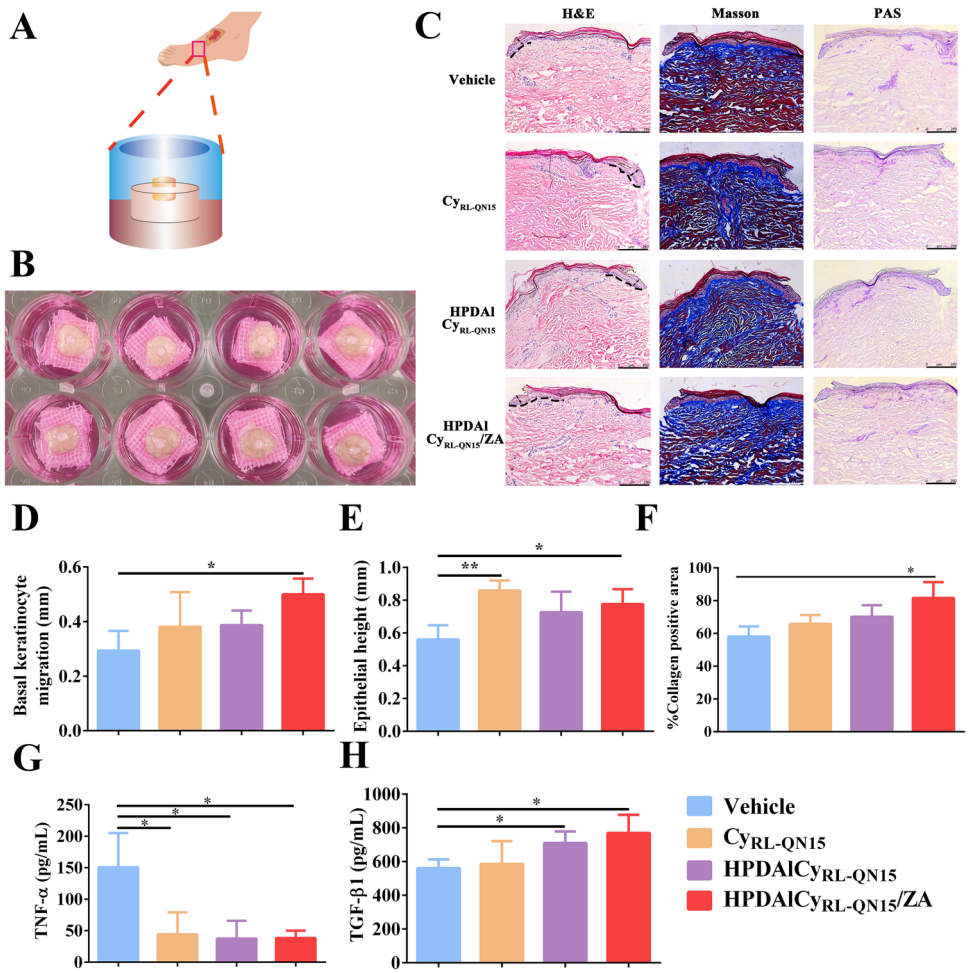

Fig. 8 Therapeutic efficacy of the HPDAlCy$_{RL-QN15}$/ZA hydrogel in ex vivo foot skin wound repair in diabetic patients. A, **B** The HPDAlCy$_{RL-QN15}$/ZA hydrogel promoted re-epithelialization in an ex vivo diabetic skin wound healing model. **C** Representative images of H&E-, Masson trichrome-, and PAS-stained wound cross-sections of isolated wound healing models treated with PBS (vehicle), Cy$_{RL-QN15}$, HPDAlCy$_{RL-QN15}$, and HPDAlCy$_{RL-QN15}$/ZA after 7 days of in vitro incubation. Scale bar: 200 μm. **D**–**F** Comparison of length, height, and collagen content of epidermal migration in wounds treated with PBS (posttreatment), Cy$_{RL-QN15}$, HPDAlCy$_{RL-QN15}$, and HPDAlCy$_{RL-QN15}$/ZA after 7 days. **G**, **H** TNF-α and TGF-β1 expression levels in diabetic patient skin after 7 days of in vitro simulated wound tissue treatment. Data represent the mean ± SD, generated from three independent experiments performed in triplicate. * and ** indicate $P < 0.05$ and $P < 0.01$, respectively.

Conclusions

The HPDAlCy$_{RL-QN15}$/ZA hydrogel accelerated the proliferation, migration, and tube formation of skin cells, regulated the secretion of cytokines, and directly scavenged free radicals and ROS. Interestingly, the HPDAlCy$_{RL-QN15}$/ZA hydrogel markedly accelerated the healing of diabetic skin wounds by promoting re-epithelialization, granulation tissue formation, collagen deposition, and angiogenesis and by reducing inflammation. Thus, the HPDAlCy$_{RL-QN15}$/ZA hydrogel can be used as a novel therapeutic strategy for the clinical treatment of chronic skin wounds.

Acknowledgements

This work was supported by grants from the National Natural Science Foundation of China (32060212, 81760648, and 82160159); Program for Innovative Research Team in the Ministry of Education of China (IRT17-R49); Major Science and Technology Project of Yunnan Province (202202AA100004); Key project from Yunnan Key Laboratory of Pharmacology for Natural Products (YKLPNP-K2301); Science and Technology Leadership Talent Project in Yunnan, China (2017HA010); Key Project of Yunnan Applied Basic Research Project-Kunming Medical University Union Foundation (202101AY070001-006); Yunnan Applied Basic Research Project Foundation (2019FB128); Project of Yunnan Applied Basic Research Project-Kunming Medical University Union Foundation (202101AY070001-036); and Innovative Team of Precise Prevention and Treatment against Metabolic Diseases of Yunnan University.

Author details

[1]Department of Anatomy and Histology & Embryology, Faculty of Basic Medical Science, Kunming Medical University, Kunming, Yunnan 650500, China. [2]School of Pharmaceutical Science & Yunnan Key Laboratory of Pharmacology for Natural Products, Kunming Medical University, Kunming, Yunnan 650500, China. [3]Key Laboratory of Chemistry in Ethnic Medicinal Resources & Key Laboratory of Natural Products Synthetic Biology of Ethnic Medicinal Endophytes, State Ethnic Affairs Commission & Ministry of Education, School of Ethnic Medicine, Yunnan Minzu University, Kunming, Yunnan

650504, China. [4]Department of Endocrinology, Affiliated Hospital of Yunnan University, Kunming, Yunnan 650021, China. [5]Department of Dermatology, First Affiliated Hospital of Kunming Medical University, Kunming, Yunnan 650500, China

Author contributions

X.Y. and Y.W. designed the project. X.Y., Y.W., Y.Y., and L.H. received financial support for the project. X.Y. and Y.W. designed and supervised the project and commented on the project. Z.F., H.S., Y.W., and C.L. structured and characterized the nanospheres. Y.W., J.N., Y.L., K.G., and Y.L. performed the in vivo experiments and analyzed the data. Y.W., Z.F., H.S., Y.W., C.L., D.S., Q.J., S.Y., and N.L. performed the SEM, FTIR, and XPS in vitro experiments and analyzed the data. Y.Y., L.H., J.N., and Y.Z. provided skin tissue samples from diabetic patients after amputation. Z.F., H.S., Y.W., and C.L. wrote the paper. All authors contributed to the discussion during the whole project. All authors read and approved the final manuscript.

Conflict of interest

The authors declare no competing interests.

Publisher's note

Supplementary information The online version contains supplementary material available at https://doi.org/10.1038/s41427-022-00444-x.

Received: 10 July 2022 Revised: 3 October 2022 Accepted: 11 October 2022.
Published online: 23 December 2022

References

1. Li, D. et al. MicroRNA-132 enhances transition from inflammation to proliferation during wound healing. *J. Clin. Invest.* **125**, 3008–3026 (2015).
2. Larouche, J., Sheoran, S., Maruyama, K., & Martino, MIM. Immune regulation of skin wound healing: Mechanisms and novel therapeutic targets. *Adv. Wound Care* **7**, 209–31 (2018).
3. Gianino, E., Miller, C. & Gilmore, J. Smart wound dressings for diabetic chronic wounds. *Bioengineering* **5**, 51 (2018).
4. Liu, Y. et al. Application of nanomaterial in hydrogels related to wound healing. *J. Nanomater.* **2022**, 1–11 (2022).
5. Ezhilarasu, H., Vishalli, D., Dheen, S. T., Bay, B.-H. & Srinivasan, D. K. Nanoparticle-based therapeutic approach for diabetic wound healing. *Nanomaterials* **10**, 1234 (2020).
6. Wang, M. et al. Nanomaterials applied in wound healing: Mechanisms, limitations, and perspectives. *J. Control Release* **337**, 236–47 (2021).
7. Weng, T. et al. Nanomaterials for the delivery of bioactive factors to enhance angiogenesis of dermal substitutes during wound healing. *Burns Trauma* **10**, tkab049 (2022).
8. Zhang, Y., Wang, Q.-Q., Zhao, Z. & Deng, C.-J. Animal secretory endolysosome channel discovery. *Zool. Res.* **42**, 141–152 (2021).
9. Cao, X. et al. Cathelicidin-OA1, a novel antioxidant peptide identified from an amphibian, accelerates skin wound healing. *Sci. Rep.* **8**, 943 (2018).
10. Wang, Y. et al. Discovery of a novel short peptide with efficacy in accelerating the healing of skin wounds. *Pharm. Res.* **163**, 105296 (2021).
11. Song, Y. et al. A short peptide potentially promotes the healing of skin wound. *Biosci. Rep.* **39**, BSR20181734 (2019).
12. Wu, J. et al. A frog cathelicidin peptide effectively promotes cutaneous wound healing in mice. *Biochem. J.* **475**, 2785–2799 (2018).
13. Murray, R. Z., West, Z. E., Cowin, A. J. & Farrugia, B. L. Development and use of biomaterials as wound healing therapies. *Burns Trauma* **7**, s41038–018-0139-7 (2019).
14. Wang, C. et al. Engineering bioactive self-healing antibacterial exosomes hydrogel for promoting chronic diabetic wound healing and complete skin regeneration. *Theranostics* **9**, 65–76 (2019).
15. Huang, R., Hu, J., Qian, W., Chen, L. & Zhang, D. Recent advances in nano-therapeutics for the treatment of burn wounds. *Burns Trauma* **9**, tkab026 (2021).
16. Zheng, Z. et al. A cannabidiol-containing alginate based hydrogel as novel multifunctional wound dressing for promoting wound healing. *Biomater. Adv.* **134**, 112560 (2021).
17. Zhang, M. et al. Zn(2+)-loaded TOBC nanofiber-reinforced biomimetic calcium alginate hydrogel for antibacterial wound dressing. *Int. J. Biol. Macromol.* **143**, 235–242 (2020).
18. Lin, P. H. et al. Zinc in wound healing modulation. *Nutrients* **10**, 16 (2017).
19. Sun, H. et al. Hollow polydopamine nanoparticles loading with peptide RL-QN15: A new pro-regenerative therapeutic agent for skin wounds. *J. Nanobiotechnol.* **19**, 304 (2021).
20. Ou, Q. et al. More natural more better: Triple natural anti-oxidant puerarin/ferulic acid/polydopamine incorporated hydrogel for wound healing. *J. Nanobiotechnol.* **19**, 237 (2021).
21. Bordon, K. C. F. et al. From animal poisons and venoms to medicines: Achievements, challenges and perspectives in drug discovery. *Front. Pharm.* **11**, 1132 (2020).
22. Yang, X., Wang, Y., Wu, C. & Ling, E. A. Animal venom peptides as a treasure trove for new therapeutics against neurodegenerative disorders. *Curr. Med. Chem.* **26**, 4749–4774 (2019).
23. Li, C., Wang, J., Zhao, M., Zhang, S. & Zhang, Y. Toll-like receptor 4 antagonist FP7 alleviates lipopolysaccharide-induced septic shock via NF-kB signaling pathway. *Chem. Biol. Drug Des.* **97**, 1151–1157 (2021).
24. Nguyen, L. T. et al. Serum stabilities of short tryptophan- and arginine-rich antimicrobial peptide analogs. *PloS One.* **5**, e12684 (2010).
25. Fu, Y. et al. Amphibian-derived peptide homodimer promotes regeneration of skin wounds. *Biomed. Pharmacother.* **146**, 112539 (2022).
26. Chen, X. et al. Preparation and application of quaternized chitosan- and AgNPs-base synergistic antibacterial hydrogel for burn wound healing. *Molecules* **26**, 4037 (2021).
27. Wang, X. et al. Preparation of antimicrobial hyaluronic acid/quaternized chitosan hydrogels for the promotion of seawater-immersion wound healing. *Front. Bioeng. Biotechnol.* **7**, 360 (2019).
28. Wu, D. et al. Exosomes derived from bone mesenchymal stem cells with the stimulation of Fe_3O_4 nanoparticles and static magnetic field enhance wound healing Through Upregulated miR-21-5p. *Int. J. Nanomed.* **15**, 7979–7993 (2020).
29. Shalin, S. C., Ferringer, T. & Cassarino, D. S. PAS and GMS utility in dermatopathology: Review of the current medical literature. *J. Cutan. Pathol.* **47**, 1096–1102 (2020).
30. Ueck, C. et al. Comparison of in-vitro and ex-vivo wound healing assays for the investigation of diabetic wound healing and demonstration of a beneficial effect of a triterpene extract. *PloS One* **12**, e0169028 (2017).
31. Gherardini, J., van Lessen, M., Piccini, I., Edelkamp, J. & Bertolini, M. Human wound healing ex vivo model with focus on molecular markers. *Methods Mol. Biol.* **2154**, 249–254 (2020).
32. Stone, R. II, Wall, J. T., Natesan, S. & Christy, R. J. PEG-plasma hydrogels increase epithelialization using a human ex vivo skin model. *Int. J. Mol. Sci.* **19**, 3156 (2018).
33. Yang, X., Lee, W. H. & Zhang, Y. Extremely abundant antimicrobial peptides existed in the skins of nine kinds of Chinese odorous frogs. *J. Proteome Res.* **11**, 306–319 (2012).
34. Li, X. et al. OM-LV20, a novel peptide from odorous frog skin, accelerates wound healing in vitro and in vivo. *Chem. Biol. Drug Des.* **91**, 126–136 (2018).
35. Hoti, G. et al. Effect of the cross-linking density on the swelling and rheological behavior of ester-bridged β-cyclodextrin nanosponges. *Materials* **14**, 478 (2021).
36. Qu, J. et al. Antibacterial adhesive injectable hydrogels with rapid self-healing, extensibility and compressibility as wound dressing for joints skin wound healing. *Biomaterials* **183**, 185–199 (2018).
37. Su, J., Li, J., Liang, J., Zhang, K. & Li, J. Hydrogel preparation methods and biomaterials for wound dressing. *Life* **11**, 1016 (2021).
38. Zhang, M. et al. Alginate-chitosan oligosaccharide-ZnO composite hydrogel for accelerating wound healing. *Carbohydr. Polym.* **266**, 118100 (2021).
39. Aitcheson, S. M., Frentiu, F. D., Hurn, S. E., Edwards, K. & Murray, R. Z. Skin wound healing: Normal macrophage function and macrophage dysfunction in diabetic wounds. *Molecules* **26**, 4917 (2021).

40. Wu, Y. et al. A spatiotemporal release platform based on pH/ROS stimuli-responsive hydrogel in wound repairing. *J. Control Release* **341**, 147–165 (2022).
41. Qi, Y. et al. A thermoreversible antibacterial zeolite-based nanoparticles loaded hydrogel promotes diabetic wound healing via detrimental factor neutralization and ROS scavenging. *J. Nanobiotechnol.* **19**, 414 (2021).
42. Liang, Y., He, J. & Guo, B. Functional hydrogels as wound dressing to enhance wound healing. *ACS Nano* **15**, 12687–12722 (2021).
43. Wang, K. et al. Exosomes laden self-healing injectable hydrogel enhances diabetic wound healing via regulating macrophage polarization to accelerate angiogenesis. *Chem. Eng. J.* **430**, 132664 (2022).
44. Jia, J. et al. AP-1 transcription factor mediates VEGF-induced endothelial cell migration and proliferation. *Microvasc. Res.* **105**, 103–108 (2016).
45. Liang, Y. et al. pH/Glucose dual responsive metformin release hydrogel dressings with adhesion and self-healing via dual-dynamic bonding for athletic diabetic foot wound healing. *ACS Nano* **16**, 3194–3207 (2022).
46. Chen, J. et al. Antibacterial adhesive self-healing hydrogels to promote diabetic wound healing. *Acta Biomater.* **146**, 119–130 (2022).
47. Chen, K. et al. Injectable melatonin-loaded carboxymethyl chitosan (CMCS)-based hydrogel accelerates wound healing by reducing inflammation and promoting angiogenesis and collagen deposition. *J. Mater. Sci. Technol.* **63**, 236–245 (2021).